HAL
open science

A New Algorithm for Synchrosqueezing: With an Application to Multicomponent Signals Sampling and Denoising

Sylvain Meignen, Thomas Oberlin, Steve Mclaughlin

To cite this version:

Sylvain Meignen, Thomas Oberlin, Steve Mclaughlin. A New Algorithm for Synchrosqueezing: With an Application to Multicomponent Signals Sampling and Denoising. 2012. hal-00667190

HAL Id: hal-00667190

https://hal.science/hal-00667190v1

Preprint submitted on 7 Feb 2012

HAL is a multi-disciplinary open access archive for the deposit and dissemination of scientific research documents, whether they are published or not. The documents may come from teaching and research institutions in France or abroad, or from public or private research centers.

L'archive ouverte pluridisciplinaire **HAL**, est destinée au dépôt et à la diffusion de documents scientifiques de niveau recherche, publiés ou non, émanant des établissements d'enseignement et de recherche français ou étrangers, des laboratoires publics ou privés.

A New Algorithm for Synchrosqueezing: With an Application to Multicomponent Signals Sampling and Denoising

Sylvain Meignen
IDCOM Laboratory,
University of Edinburgh Scotland, UK
Tel:0044-131-650-5659
FAX:0044 131 650 6554
email: sylvain.meignen@imag.fr
Thomas Oberlin
Jean Kuntzmann Laboratory,
University of Grenoble, France
Tel:0033-4-76-51-45-61
email: thomas.oberlin@imag.fr
Steve McLaughlin FIEEE,
School of Engineering and Physical Sciences,
Heriot-Watt University, Edinburgh Scotland, UK
Tel 0044 131 451 4127
email: s.mclaughlin@hw.ac.uk

Abstract- In this paper, we address the practical implementation of the synchrosqueezing method. The emphasis is placed on the importance of the wavelet choice and we propose a novel algorithm based on a two step strategy: a mode detection step followed by a reconstruction step. Simulations will illustrate how the proposed procedure compares favorably with empirical mode decomposition and other related methods in terms of mode-mixing. We conclude the paper by studying the sensitivity of the synchrosqueezing to sampling and an application to signal denoising.

Keywords-SynchroSqueezing, Wavelets, EMD, Time-Frequency, Sampling, Denoising
EDICS Category: DSP-TFSR

I. Introduction

Audio signals are commonly modelled as a sum of AM/FM components with slowly varying amplitude and instantaneous frequency [13]. Consequently, the retrieval of the components of a multicomponent signal is a central issue in many audio processing problems. The most commonly used techniques to carry out the retrieval are time-frequency or time-scale based signal representations. For the former, spectrogram reassignment techniques [3], reconstruction based on l_1 minimization of the ambiguïty function associated with the Wigner-Ville distribution [6], synchrosqueezing using the short time Fourier transform [14] or Fourier ridges [2] have all been successfully used. For the latter, i.e., time-scale representations, wavelet ridges have also proven to be very efficient [10] [9]. In [9], the emphasis is put on the importance of the wavelet choice with regard to the ridge representation. Synchrosqueezing techniques have also been developed within the wavelet framework [4]. The main difference between the short time Fourier and wavelet representations is that the latter is more demanding in terms of the frequency separation of high frequency components.

In this paper, we will first discuss the practical implementation of the synchrosqueezing method (SM) and then show how it enables us to find out a relevant non uniform sampling set for the signal, i.e. preserving its essential frequency characteristics, and finally how it can be used for signal denoising. The layout of the paper is the following. In section II, we recall some notation that are useful to describe the SM. Then, we restate the main theoretical related results [4] with a practical implementation recently proposed by Brevdo et *al.* in [1] (section III). While recalling these results on the SM in a wavelet framework, we also point out that they can easily be adapted to a short time Fourier transform (STFT) framework. In this regard, we propose a novel restatement of the SM in a STFT framework that is consistent with the reconstruction formula associated with this transform. A fundamental issue in synchrosqueezing is the wavelet choice; a poor wavelet representation inevitably leads to a poor synchrosqueezing transform. Therefore, in section IV, we focus on the difference between applying the wavelet transform to pure harmonic or to multicomponent signals. We deduce from this study that a good wavelet representation for pure harmonic signals is only related to the frequency support of the wavelet while that of multicomponent signals is related to the ratio between the first and the second derivatives of the phase (for a multicomponent signal made of frequency modulated signals). When such a ratio is high, we show that moving the frequency center of the wavelet towards zero improves the quality of the wavelet representation. Bearing in mind these elements, we propose a novel algorithm for the implementation of the SM in section V. It is based on a mode detection step followed by a reconstruction step that takes

into account the particular structure of the wavelet transform of multicomponent signals. The numerical simulations of section VI show that the proposed reconstruction algorithm provides good mode separation and compares favorably to *empirical mode decomposition* (EMD) [8] and other existing algorithms related to the implementation of the synchrosqueezing method [1]. Finally, we conclude the paper by proposing a potential use of the synchrosqueezing method to determine a relevant sampling strategy for multicomponent signals analysis and also by showing that the algorithm we propose for synchrosqueezing naturally provides a very efficient denoising algorithm that outperforms wavelet thresholding technique for the multicomponent signals studied.

II. Notation and Definitions

We denote by $\hat{f}$ the Fourier transform of f, defined using the following normalization:

$$\hat{f}(\xi) \quad = \quad \int_{\mathbb{R}} f(x) e^{-2i\pi\xi x} dx. \tag{1}$$

Let f be a tempered distribution, and g be in the Schwartz class $\mathcal{S}(\mathbb{R})$, such that $\hat{g}$ is compactly supported with its support centered in 0 ; the short time Fourier transform of f is defined as:

$$V_f(\eta, t) := \int_{-\infty}^{+\infty} f(x) g(x-t) e^{-2i\pi\eta(x-t)} dx. \tag{2}$$

For $f \in L^2(\mathbb{R})$, we define the continuous wavelet transform:

$$W_f(a,t) \quad = \quad \int_{\mathbb{R}} f(x) \frac{1}{a} \overline{\Psi(\frac{x-t}{a})} dx, \tag{3}$$

where $\Psi \in L^2(\mathbb{R})$ is a function called a wavelet satisfying the condition $\int_0^{+\infty} \frac{\left|\hat{\Psi}(\xi)\right|^2}{\xi} d\xi < +\infty$. The wavelet is said to be analytic if $\hat{\Psi}(\xi) = 0$, $\xi \leq 0$. A particular class of analytic wavelets are those admitting a unique peak frequency:

$$\xi_\Psi = \underset{\xi}{\text{argmax}} \left|\hat{\Psi}(\xi)\right|. \tag{4}$$

As an illustration, let us consider the *bump wavelet* defined

$$\hat{\Psi}(\xi) \quad = \quad e^{1 - \frac{1}{1-(\frac{\xi-\mu}{\sigma})^2}} \chi_{[\mu-\sigma, \mu+\sigma]}, \tag{5}$$

which admits a peak frequency $\xi_\Psi = \mu$.

III. Synchrosqueezing Basics

In what follows, we investigate the retrieval of the components f_k of a multicomponent signal f with duration $T = n\Delta t$, (Δt being the time span), defined by:

$$f(t) = \sum_{k=1}^{K} A_k(t)\cos(2\pi\phi_k(t)) = \sum_{k=1}^{K} f_k(t), \tag{6}$$

where $A_k(t) > 0$. Note that one can associate with f its *ideal TF distribution* $\rho(t,\xi) = \sum_{k=1}^{K} A_k^2(t)\delta(\xi - \phi_k'(t))$. The problem can be viewed from two perspectives. The first consists of computing an approximation of the modes, either by using EMD [8] or via wavelet projections [11] and then deriving the Hilbert spectrum of f to obtain an approximation of the ideal TF distribution. The second, used by the SM, which we will study hereafter, consists in computing a quantity $\hat{\omega}$ which is based on assessing the frequency content of the signal f in the time-scale space and which is subsequently used to weight the wavelet transform of f and finally retrieve the modes f_k.

A. Theoretical Aspects

For the the sake of consistency, we recall some theoretical results stated in [4]. These were established for a signal f defined as a superposition of *intrinsic-mode-type* functions(IMT):

Definition 1: A function $f : \mathbb{R} \to \mathbb{R}$ is said to be a superposition of well-separated IMTs with accuracy ϵ and separation d, the set of which is denoted by $\mathcal{A}_{\epsilon,d}$ in the sequel, if there exists a finite K such that $f(t) = \sum_{k=1}^{K} f_k(t) = \sum_{k=1}^{K} A_k(t)\cos(2\pi\phi_k(t))$, where all the f_k are $\epsilon-$IMTs satisfying:

$$\begin{cases} \phi_k'(t) > \phi_{k-1}'(t) \\ |\phi_k'(t) - \phi_{k-1}'(t)| \geq d(\phi_{k-1}'(t) + \phi_k'(t)). \end{cases}$$

An IMT is defined as follows:

Definition 2: A continuous function $f : \mathbb{R} \to \mathbb{R} \in L^\infty(\mathbb{R})$ is said to be of the *intrinsic-mode-type (IMT) with accuracy* ϵ if $f(t) = A(t)\cos(2\pi\phi(t))$ with A and ϕ satisfying the following properties:

$$\begin{aligned} & A \in C^1(\mathbb{R}) \bigcap L^\infty(\mathbb{R}),\ \phi \in C^2(\mathbb{R}) \\ & \inf_{t\in\mathbb{R}} \phi'(t) > 0,\ \sup_{t\in\mathbb{R}} \phi'(t) < \infty,\ \sup_{t\in\mathbb{R}} |\phi''(t)| < \infty \\ & |A'(t)|, |\phi''(t)| \leq \epsilon|\phi'(t)|,\ \forall t \in \mathbb{R} \end{aligned}$$

Let us consider the following description of the frequency representation of f in the time-scale space:

$$\hat{\omega}(a,t) \quad = \quad \frac{\partial_t W_f(a,t)}{2i\pi W_f(a,t)}, \tag{7}$$

which is only defined for a non zero wavelet coefficient. The main theorem defining the synchrosqueezing method was detailed in [4] and is as follows:

Theorem 1: Let f be a function in $\mathcal{A}_{\epsilon,d}$ and set $\tilde{\epsilon} = \epsilon^{1/3}$. Select a function h in C_c^∞ with $\int h(t)dt = 1$, and a wavelet Ψ in $\mathcal{S}(\mathbb{R})$ such that its Fourier transform $\hat{\Psi}$ is supported in $[1-\Delta, 1+\Delta]$, with $\Delta < d/(1+d)$. Consider the function obtained by synchrosqueezing W_f, with threshold $\tilde{\epsilon}$ and accuracy δ, i.e.

$$S^\delta_{f,\tilde{\epsilon}}(t,\omega) = \int_{A_{\tilde{\epsilon},f}(b)} W_f(a,t)\frac{1}{\delta}h(\frac{\omega - \hat{\omega}(a,t)}{\delta})\frac{da}{a},$$

where $A_{\tilde{\epsilon},f} = \{a \in \mathbb{R}^+; |W_f(a,t)| > \tilde{\epsilon}\}$. Then provided ϵ is sufficiently small, the following condition holds:

- $|W_f(a,t)| > \tilde{\epsilon}$ only when for some $k \in \{1, \cdots, K\}$, $(a,t) \in Z_k := \{(a,t); |a\phi_k'(t) - 1| < \Delta\}$.
- For each $k \in \{1, \cdots, K\}$, and for each pair $(a,t) \in Z_k$, for which holds $|W_f(a,t)| > \tilde{\epsilon}$, we have $|\hat{\omega}(a,t) - \phi_k'(t)| \leq \tilde{\epsilon}$
- Moreover, for each $k \in \{1, \cdots, K\}$, there exists a constant C, such that, for any t in $\mathbb{R}$,

$\left|\lim_{\delta\to 0} \frac{2}{C_\Psi}\mathcal{R}e\left[\int_{B_{\tilde{\epsilon},k}} S^\delta_{f,\tilde{\epsilon}}(t,\omega)d\omega\right] - A_k(t)\cos(2\pi\phi_k(t))\right| \leq C\tilde{\epsilon}$, where $C_\Psi = \int_0^\infty \overline{\hat{\Psi}(\xi)}\frac{d\xi}{\xi}$ and $B_{\tilde{\epsilon},k} := \{\omega,\ |\omega - \phi_k'(t)| < \tilde{\epsilon}\}$.

<u>Remark:</u> This version of the theorem differs slightly from the original since here we deal with real signals as opposed to complex and a different normalization of the wavelet transform is adopted than that originally proposed.

To retrieve the modes f_k the synchrosqueezing method uses the following reconstruction formula: $f(t) = 2\mathcal{R}e\left[C_\Psi^{-1}\int_0^\infty W_f(a,t)\frac{da}{a}\right]$, and then, as stated above, it suffices to sum up considering only the scales a in $A_{\tilde{\epsilon},f}(t)\bigcap\{a : |a\phi_k'(t) - 1| < \Delta\}$. This approach is valid only for small ϵ, we may ponder the following: what happens at larger ϵ and does the synchrosqueezing method lead to good results in such circumstances. This point is dealt with in section VI where a particular emphasis is put on the wavelet choice.

B. Practical Implementation

We recall a practical implementation proposed by Brevdo et *al.* in [1] which is based on the theoretical results described above. To highlight the frequency components involved in the reconstruction of $f(t)$, one defines a binning of the frequency $\{\omega_l\}_{l=0}^\infty$ and then $\mathcal{W}_l = [\frac{\omega_l + \omega_{l-1}}{2}, \frac{\omega_l + \omega_{l+1}}{2}]$. With this in mind, the synchrosqueezing operator corresponds to: $T_f(\omega_l, t) = \int_{a:|\hat{\omega}(a,t)|\in\mathcal{W}_l} W_f(a,t)\frac{da}{a}$, which satisfies $f(t) = \sum_l T_f(\omega_l, t)$. By changing variables, we can write: $T_f(\omega_l, t) = \int_{u:|\hat{\omega}(2^{u/n_v}\Delta t, t)|\in\mathcal{W}_l} W_f(2^{u/n_v}, t)\frac{\log(2)}{n_v}du$, where n_v is associated with the discretization of the scales a into $a_j = 2^{j/n_v}\Delta t$, $j = 0, \cdots, Ln_v - 1$.

Now, putting $n_a = Ln_v$, the Nyquist-Shannon theorem suggests that the maximum frequency is $\bar{\omega} = \omega_{n_a-1} = \frac{1}{2\Delta t}$ and, under a periodic assumption for the signal, the minimum is $\underline{\omega} = \omega_0 = \frac{1}{n\Delta t}$. Assuming ω varies on a log scale: $\omega_l = 2^{l\Delta\omega}\underline{\omega}$, we obtain $\Delta\omega = \frac{1}{n_a-1}\log_2(n/2)$. Consequently, a discrete version of $T_f(\omega_l, b)$ can finally be written as follows:

$$T_{d,f}(\omega_l, q) = \sum_{0\leq j\leq n_a-1, j:|\hat{\omega}(a_j, q\Delta t)|\in\mathcal{W}_l} W_f(a_j, q\Delta t)\frac{\log(2)}{n_v}. \tag{8}$$

This operator satisfies $f(q\Delta t) \approx 2\mathcal{R}e\left[C_\Psi^{-1}\sum_l T_{d,f}(\omega_l, q)\right]$. The strategy developed to retrieve the components of a multicomponent signal [1] is to proceed on a component by component basis. The idea is to find a curve $(c_q^*)_{q=0,\cdots,n-1}$, in the time-frequency plane such that it maximizes the energy while forces the modes to be smooth through a total variation term penalization and is obtained by computing the following quantity:

$$c^* = \underset{c\in\{1,\cdots,n_a\}^n}{\text{argmax}} \sum_{q=0}^{n-1}\log(|T_{d,f}(\omega_{c_q}, q)|^2) - \sum_{q=1}^{n}\lambda\Delta\omega|c_q - c_{q-1}|^2. \tag{9}$$

Note that it is assumed that the component persists for the whole signal duration, if it only persists for some part of it, the corresponding $T_{d,f}(\omega_{c_q}, q\Delta t)$ will contribute very little to the reconstruction process. When c_q^* has been found, the associated component at time $q\Delta t$ can be reconstructed by summing up $T_{d,f}(\omega_l, q)$ for l in $\mathcal{N}_q := [c_q^* - n_v/2, c_q^* + n_v/2]$ in the above formula. To find the next component, one sets $T_{d,f}(\mathcal{N}_q, q)$ to zero and restarts the minimization procedure on the remaining transform. In section V, we will propose an alternative approach to this construction which will prove to be both more accurate and computationally much less demanding.

C. An Alternative Definition Based on the Short-Time Fourier Transform

In a very similar manner, one can define the frequency content of f in the time-frequency plane from its STFT by:

$$\hat{\eta}(\eta, t) = \frac{\partial_t V_f(\eta, t)}{2i\pi V_f(\eta, t)}. \tag{10}$$

Rewriting the STFT of the signal f as: $V_f(\eta, t) := \int_{-\infty}^{+\infty} f(x+t)g(x)e^{-2i\pi\eta x}\,dx$, $V_f(\eta, t)$ can be viewed as the Fourier transform of the function $x \mapsto f(x+t)g(x)$ at frequency η. Supposing that $g(0) \neq 0$, we can write $f(t) = \frac{1}{g(0)}\int_{-\infty}^{+\infty} V_f(\eta, t)d\eta$. This reconstruction formula is very similar to the wavelet case and the same theoretical developments as in Theorem 1 can be carried out by changing the mode separation condition into $|\phi_k'(t) - \phi_{k-1}'(t)| \geq d$ [14]. This suggests creating a partition $(\mathcal{W}_l)_l$ of frequencies and writing: $S_f(\omega_l, t) = \int_{\xi:|\hat{\eta}(\eta,t)|\in\mathcal{W}_l} V_f(\eta, t)d\eta$. This approach is similar to that introduced in [14] except

that the operator used there was $\tilde{S}_f(\omega_l,t) = \int_{\xi:|\hat{\eta}(\eta,t)|\in\mathcal{W}_l} d\eta$, and was thus not consistent with the reconstruction formula.

By dividing the frequency domain linearly, that is $\underline{\omega} = \omega_{n_a-1} = \frac{1}{2\Delta t}$ and $\bar{\omega} = \omega_0 = \frac{1}{n\Delta t}$, we are lead to consider $\Delta\omega = \frac{n-2}{2n\Delta t(n_a-1)}$ and subsequently a discrete version of S_f would take the following form: $S_{d,f}(\omega_l,q) = \sum_{0\le p\le n_a-1, p:|\hat{\eta}(p\Delta\omega,q\Delta t)|\in\mathcal{W}_l} \frac{\Delta\omega}{g(0)} V_f(p\Delta\omega, q\Delta t)$.

The algorithm for component retrieval can be applied to the STFT replacing $T_{d,f}$ by $S_{d,f}$. Note that the meaning of $\mathcal{N}_q$ as defined at the end of section III-B is also different due to the change in the binning process.

IV. On the Parameters of the Synchrosqueezing Algorithm

In this section, we consider an analytic wavelet such that $\hat{\Psi}$ is compactly supported. We first introduce some approximation formulae of the wavelet transform that need to be verified for ensuring that the synchrosqueezing technique is well behaved and then we discuss the estimation of $\hat{\omega}$.

A. WT and STFT for Pure Harmonic Signals

Assume that the signal we study is composed of pure harmonic signals, that is: $f(t) = \sum_{k=1}^{K} A_k \cos(2\pi\phi_k t)$, with $\phi_{k-1} < \phi_k$. If the signal is made of a single pure harmonic component $A\cos(2\pi\phi t)$, then the wavelet transform is as follows: $W_f(a,t) = \frac{1}{2}Ae^{2i\pi\phi t}\overline{\hat{\Psi}(a\phi)}$. It is thus clear that, provided supp$(\hat{\Psi}) \subset [1-\Delta, 1+\Delta]$, we have $\omega_2(a,t) = \phi$ for all t such that $1-\Delta < a\phi < 1+\Delta \Leftrightarrow \frac{1-\Delta}{\phi} < a < \frac{1+\Delta}{\phi}$. Then a necessary condition for the synchrosqueezing to work well is for all $k > 1$: $\frac{1+\Delta}{\phi_k} < \frac{1-\Delta}{\phi_{k-1}} \Leftrightarrow \Delta < \frac{\phi_k-\phi_{k-1}}{\phi_k+\phi_{k-1}}$. In addition, following Definition 1 we assume the frequency separation obeys the following rule:$\phi_k - \phi_{k-1} \ge d(\phi_k + \phi_{k-1})$. Then it is sufficient to have $\Delta \le d$ to obtain perfect separation. Indeed, in this case, any a belongs to at most one $X_k := \{|a\phi_k - 1| < \Delta\}$, on which we have: $W_f(a,t) = \frac{1}{2}A_k e^{2i\pi\phi_k t}\overline{\hat{\Psi}(a\phi_k)}$, $W_f(a,t)$ being null outside of the union of the X_k, and then $\hat{\omega}(a,t)$ is a perfect estimator of ϕ_k.

For the STFT representation, we would assume the following frequency separation condition: $|\phi_{k-1} - \phi_k| \ge d$ for $k > 1$ and $\phi_1 \ge d/2$. As a result of the linearity of the STFT, we may write, (assuming supp $\hat{g} \subset [-d/2, d/2]$ and η in $Y_k = \{|\eta - \phi_k| \le d/2\}$): $V_f(\eta,t) = \frac{1}{2}A_k e^{i2\pi\phi_k t}\overline{\hat{g}(\eta-\phi_k)}$, which is null outside the union of the Y_k. Again, when separation is achieved, $\hat{\eta}(\eta,t)$ defined in (10) equals ϕ_k when $\eta \in Y_k$.

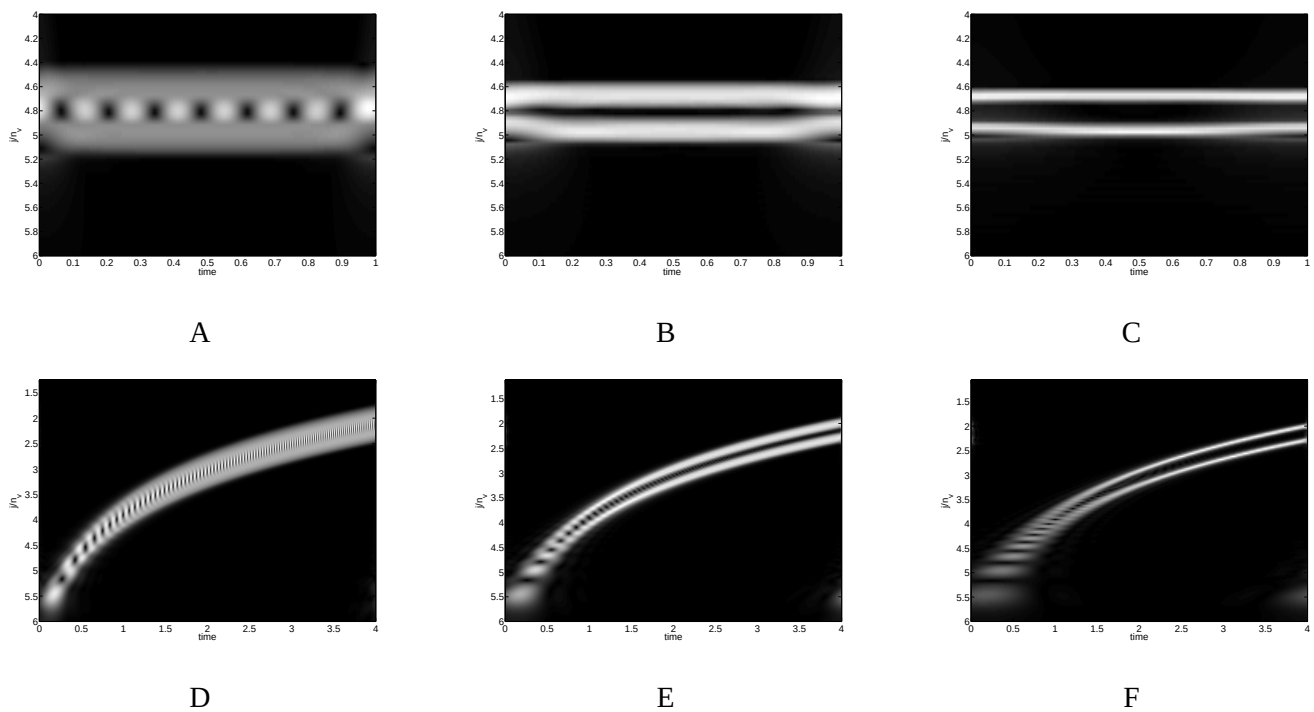

Fig. 1: From top to bottom: the modulus of the wavelet transform of the signal $\cos(2\pi * 40 * t) + \cos(2\pi * 32.72 * t)$, the modulus of the wavelet transform of $\cos(2\pi * 30 * (t+1/4)^2) + \cos(2\pi * 24.55 * (t+1/4)^2)$. analyzed with the bump wavelet with parameters $\mu = 1$ and from left to right: $\sigma = 0.2,\ 0.1,\ 0.05$.

B. WT and STFT for Multicomponent Signals

For multicomponent signals as defined in Definition 1, the study is basically the same. We still consider that supp$(\hat{\Psi}) \subset [1-\Delta, 1+\Delta]$. In such a case, one considers the following approximation of the wavelet transform:

$$W_f(a,t) \quad \approx \quad \frac{1}{2} A_k(t) e^{2i\pi\phi_k(t)} \overline{\hat{\Psi}(a\phi_k'(t))}, \tag{11}$$

for any given pair (a,t) satisfying $1-\Delta < a\phi_k'(t) < 1+\Delta$. This requires that for all $k > 1$ and all t: $\frac{1+\Delta}{\phi_k'(t)} < \frac{1-\Delta}{\phi_{k-1}'(t)} \Leftrightarrow \Delta < \frac{\phi_k'(t)-\phi_{k-1}'(t)}{\phi_k'(t)+\phi_{k-1}'(t)}$. As the frequency separation obeys for all t the rule given in Definition 1: $\phi_k'(t) - \phi_{k-1}'(t) \geq d(\phi_k'(t) + \phi_{k-1}'(t))$, we can deduce that the approximation makes sense as soon as $\Delta < d$.

For the case of the STFT representation, we would assume the frequency separation given by the rule: $|\phi_{k-1}'(t) - \phi_k'(t)| \geq d$, for $k > 1$ and $\phi_1'(t) \geq d/2$. Also, as supp$(\hat{g}) \subset [-d/2, d/2]$, and considering any

given pair (η, b) such that $|\eta - \phi_k'(t)| \leq d/2$, we have the following approximation:

$$V_f(\eta, t) \approx \frac{1}{2} A_k(t) e^{i2\pi\phi_k(t)} \overline{\hat{g}(\eta - \phi_k'(t))}. \tag{12}$$

Note that this upper bound for Δ in the wavelet approximation is larger than that derived in [4], which stated that the separation was only possible if $\Delta < \frac{d}{1+d}$. The key difference is that the inequalities used in [4] were $a\phi_k'(t) - a\phi_{k-1}'(t) \leq (1+\Delta) - (1-\Delta) = 2\Delta$ and $a\phi_k'(t) + a\phi_{k-1}'(t) \geq 2(1-\Delta)$ which are too sharp since there is no t which can attain these bounds simultaneously.

To be valid, the approximations described in (11) and (12) both require that ϵ, (introduced in Definition 2), be sufficiently small. The fundamental difference between a signal made of pure harmonics and a multicomponent signal is the dependence of the latter on ϵ. To illustrate this we consider a sum of two cosines with close frequencies, and a sum of two linear chirps with close instantaneous frequencies, such that both signals satisfy the condition $\phi_1'(t) - \phi_2'(t) = \frac{1}{10}(\phi_1'(t) + \phi_2'(t))$. We analyze these signals with a bump wavelet (see definition (5)). We take $\xi_\Psi = \mu = 1$ and we take $\Delta = \sigma$ equal to either 0.2, 0.1 or 0.05. For the multicomponent signal and contrary to what happens for a signal made of pure harmonics, when $\sigma = 0.05$, in spite the frequency separation condition is verified, the wavelet representation is poor meaning that the approximation (11) is inaccurate (compare Figure 1 C and F). With reference to the study by Mallat on wavelet ridges, ([10], p.102), and recalling that the wavelet frequency center is denoted by ξ_Ψ, (which equals 1 in the example above), the second order terms in the approximation (11) would be negligible only if:

$$\frac{\xi_\Psi^2}{|\phi_k'(t)|^2} \frac{|A_k''(t)|}{|A_k(t)|} << 1 \quad \text{and } \xi_\Psi^2 \frac{|\phi_k''(t)|}{|\phi_k'(t)|^2} << 1, \tag{13}$$

provided $\frac{\xi_\Psi}{|\phi_k'(t)|} \frac{|A_k'(t)|}{|A_k(t)|} \leq 1$. We are now going to show that the quality of the approximation (11) greatly influences that of the wavelet transform. The constraints described in (13) when applied to an IMT imply that ϕ is such that $\phi'(t) \geq \xi_\Psi \epsilon$, provided that $\frac{\xi_\Psi}{|\phi'(t)|} \frac{|A'(t)|}{|A(t)|} \leq 1$, which is true when $\frac{\xi_\Psi \epsilon}{A(t)} \leq 1$, or equivalently $A(t) \geq \xi_\Psi \epsilon$. If we assume that both A and ϕ' are bounded below, the wavelet decomposition leads to better results by taking ξ_Ψ smaller when ϵ is large. Note also, that, if we analyze the signal with a wavelet Ψ such that $\text{supp}(\hat{\Psi}) \subset [\xi_\Psi - \Delta, \xi_\Psi + \Delta]$, then Δ needs to be inferior to $\xi_\Psi d$ to ensure the frequency separation condition. Thus, to take a small value for ξ_Ψ when ϵ is large as suggested by the constraints (13) applied to an IMT, requires that the Fourier transform of the wavelet be better localized since we must have $\Delta \leq \xi_\Psi d$.

As an illustration consider the wavelet transform of $\cos(2\pi * 30 * (t + 1/4)^2)$. The first inequality of (13) is always satisfied in the present case, while the second may not be verified when ξ_Ψ is chosen

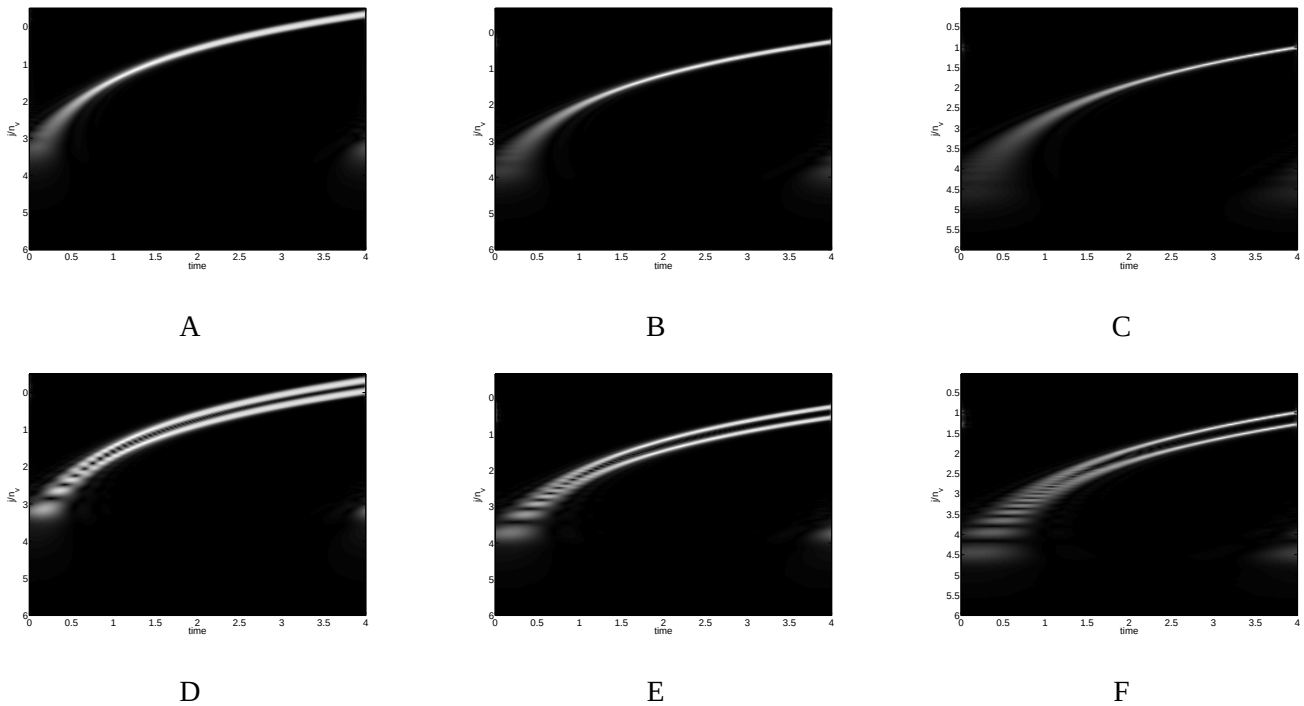

Fig. 2: From top to bottom: modulus of the wavelet transform of $\cos(2\pi * 30 * (t + 1/4)^2)$ and that of $\cos(2\pi * 30 * (t + 1/4)^2) + \cos(2\pi * 24.55 * (t + 1/4)^2)$. From left to right: for $\sigma = 0.02$ and $\mu = 0.2$, 0.3, 0.5

too large. Indeed, in the case studied, since $\Phi''(t)/\Phi'(t)$ is decreasing with t we get $\epsilon = 4$ and, as $\Phi'(t)$ equals 2 in 0 and is increasing, we need to take $\xi_\Psi \leq 0.5$, for the second inequality of (13) to be satisfied. Note the role of the wavelet frequency center on the decomposition, we analyze the signal with the bump wavelet considering $\sigma = 0.02$, μ being either equal to 0.2, 0.3 or to 0.5. We have taken $\sigma = 0.02$ in the simulations to ensure that $\Delta \leq \xi_\Psi d$ even when $\xi_\Psi = F_c = 0.2$. In Figures 2 A to C we see that, on the one hand, we have a better wavelet representation for small ξ_Ψ when t is small but this improvement is to the detriment of the representation for larger t. Then when one considers a signal $\cos(2\pi * 30 * (t + 1/4)^2) + \cos(2\pi * 24.55 * (t + 1/4)^2)$ made of two linear chirps, we notice that a better wavelet representation of each of the linear chirp results in less interference as confirmed by comparison between Figures 2 D to F. To conclude, for signals made of pure harmonics what matters is how well the wavelet transform separates the modes while for multicomponent signals the strength of the modulation ϵ must also be taken into account in the wavelet choice. Later on we will use the

previous remark regarding the location of the frequency center of the wavelet to improve the results of the synchrosqueezing method for large ϵ.

Remark: if the STFT was used instead, the second order terms in (12) would be negligible if: $\frac{|A_k''(t)|}{|A_k(t)|} << 1, |\phi_k''(t)| << 1$, provided $\frac{|A_k'(t)|}{|A_k(t)|} \leq 1$.

C. Estimation of $\hat{\omega}$ on Signals Made of Pure Harmonics

Before considering a signal made of pure harmonics, let us analyze the computation of $\hat{\omega}(a,t)$ for a single pure harmonic signal, $A\cos(2\pi\phi t)$. In this case, whatever the analytic wavelet used for analysis, $\hat{\omega}(a,t) = \phi$ for any a such that $\hat{\Psi}(a\phi) \neq 0$. We first start by telling an argument that precludes the use of a wavelet whose Fourier transform is not compactly supported. Indeed, in such a case, even if $\hat{\Psi}(a\phi)$ is extremely small, one still has $\hat{\omega}(a,t) = \phi$ because $\hat{\Psi}(a\phi)$ is on both the numerator and denominator of $\hat{\omega}(a,t)$). Now, if a signal consisting of pure harmonics as defined in section IV-A is considered a consequence of the previous remark is that the regions $R_k = \{(a,t), \hat{\omega}(a,t) = \phi_k\}$ are ill-defined. However analyzing the signal with a wavelet admittting a compactly supported wavelet does not completely resolve the problem of the computation of $\hat{\omega}(a,t)$ and a threshold still needs to be applied to the wavelet coefficients to get something relevant. To illustrate this point, let us consider $\cos(2\pi * 40 * t) + \cos(2\pi * 32.72 * t)$ for which we compute $\hat{\omega}$ using $\widehat{W_f}(a,\xi) = \hat{f}(\xi)\hat{\Psi}(a\xi)$, remarking that $\widehat{\partial_t W_f}(a,\xi) = 2i\pi\xi\widehat{W_f}(a\xi)$ and finally inverting these quantities as in [1]. The wavelet we use is again the bump wavelet ($\mu = 1$, $\sigma = 0.05$ ensuring the frequency separation condition). Due to numerical considerations instead of computing the true $\hat{\omega}(a,t)$, we set it to zero whenever $|W_f(a,t)| < \gamma$, γ being a certain threshold. In what follows, we will call $\hat{\omega}_s$ the corresponding quantity and we now study its evolution with γ . Note that for the signal studied, the maximum of the wavelet transform is $1/2$ which means that γ should be significantly smaller than this value. Figure 3 displays, for a fixed t, $\hat{\omega}_s(a,t)$ as a function of γ (which is in that case independent of the choice for t). It appears that one needs to take γ large to be able to associate $\hat{\omega}_s$ with the presence of two distinct modes but then the numerical value obtained for $\hat{\omega}_s(a,t)$ is different from the theoretical expectation. Indeed, it should be equal to ϕ_k for all a in $[\frac{1-\Delta}{\phi_k}, \frac{1+\Delta}{\phi_k}]$ which is not exactly the case. For instance, the mean square error (measured in dB) relative to the evaluation of $\hat{\omega}$ by $\hat{\omega}_s$ and taking $\gamma = 2.10^{-2}$ is 9.56 dB. This inaccuracy means that the summation (8) used to define the synchrosqueezing transform is biased due to the error in the computation of $\hat{\omega}$. To investigate whether the estimation error could be improved by analyzing the signal with a wavelet whose Fourier transform decays slower than that of the bump wavelet, we compute $\hat{\omega}_s(a,t)$ with the following

Shannon wavelet defined by: $\hat{\Psi}(\xi) = \chi_{[\mu-\sigma,\mu+\sigma]}$. Doing so, however we do not obtain any significant improvments. For instance, when $\gamma = 2.10^{-2}$, we obtain a mean square error relative to the evaluation of $\hat{\omega}$ equal to 6.30 dB which is even worse than in the case of the bump wavelet using the same parameters. It appears that the lack of precision in the estimation of $\hat{\omega}$ is related to the fact that the Fourier transform of a discretized cosine function is not strictly speaking a Dirac distribution. Consequently, even in simple cases, a large γ is required for a meaningful $\hat{\omega}_s$ but large wavelet coefficients are not dealt with in the reconstruction formula (8), leading to large reconstruction errors. In the new algorithm we propose in the next section for mode reconstruction, we will remove the need for the estimation of $\hat{\omega}$.

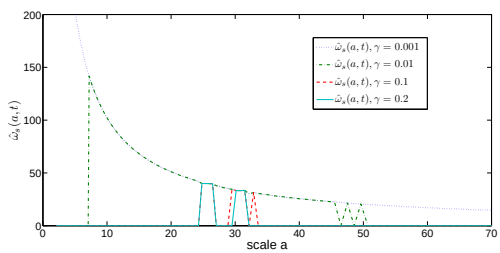

Fig. 3: $\hat{\omega}_s(a,t)$ computed using different threshold γ for the signal $\cos(2\pi * 40 * t) + \cos(2\pi * 32.72 * t)$ using the bump wavelet with $\mu = 1$ and $\sigma = 0.05$

V. A NEW ALGORITHM FOR THE RETRIEVAL OF MODES IN A SYNCHROSQUEEZING FRAMEWORK

The algorithm we propose to retrieve the modes is based on three distinct steps: a determination of the number of modes step, an optimal wavelet threshold computation step and a modes reconstruction step based on the first two steps.

A. Detection of the Number of Modes

To get rid of the estimation $\hat{\omega}$ we first remark that the latter is basically non zero as soon as $W_f(a,t)$ is above a certain threshold. In that context, given a threshold γ, it is natural to introduce the following sets:

$$C_f(\gamma,t) = \{j, |W_f(a_j,t)| < \gamma \text{ and } |W_f(a_{j+1},t)| > \gamma\}. \tag{14}$$

Note that the normalization of the wavelet transform we use is necessary to give sense to the above set. Indeed, if we consider a sum of pure harmonics with the same amplitude then the wavelet transform at the

frequencies of interest should also have the same amplitude. In our context and given γ, we will consider that a mode for a given time t is associated with a set of successive scales a_j such that $|W_f(a_j,t)| > \gamma$, and consequently with some index j_0 in $C_f(\gamma,t)$. With that in mind and given a range Γ for γ, we compute an estimation of the number of modes as follows:

$$N_f(\Gamma) \quad = \quad \text{round}(\underset{t,\gamma\in\Gamma}{\text{mean}}\,\#(C_f(\gamma,t))), \tag{15}$$

where $\#X$, denotes the cardinality of X. The quantity $N_f(\Gamma)$ corresponds to the average number of modes over all times t and γ in Γ. To give an insight into how Γ should be chosen, we shall remark that as the Fourier transforms of the wavelets are normalized to one at their peak frequencies, then refering to (11) at the corresponding scale corresponding to let us say the kth mode, the modulus of the wavelet transform almost equals $1/2A_k(t)$. Thus, the set Γ admits as upper bound $1/2\max_k \|A_k\|_\infty$. Furthermore, the maximal value in the set Γ should not be taken too small so that the true number of modes can indeed be detected.

B. Wavelet Threshold

In our determination of the relevant wavelet threshold γ, we favor a value of that parameter that leads to at least the expected number of modes for each t. As we will see later, it is only worth focusing on cases where the number of detected modes at least equals the expected one. We thus first seek a value $\hat{\gamma}$ of γ as follows:

$$\hat{\gamma} = \underset{\gamma}{\text{argmin}}\left\{\text{mean}(\#(C_f(\gamma,t)) - N_f(\Gamma)),\ .s.t.\ \forall t\ \#(C_f(\gamma,t)) \geq N_f(\Gamma)\right\}. \tag{16}$$

This corresponds to the value of γ that on average gives $\#(C_f(\gamma,t))$ the closest to $N_f(\Gamma)$, imposing that, for each t, $\#(C_f(\gamma,t))$ be larger than $N_f(\Gamma)$. When $\hat{\gamma}$ exists, to consider such a value ensures that for each t, we have detected at least as many modes as the expected number $N_f(\Gamma)$.

However, in some instances, especially when the modes we try to extract interfere, such a value $\hat{\gamma}$ may not exist, in which case we will alternatively use:

$$\bar{\gamma} = \underset{\gamma}{\text{argmin}}\left\{\text{mean}(\#(C_f(\gamma,t)) - N_f(\Gamma))\right\}, \tag{17}$$

which, contrary to $\hat{\gamma}$ always exists. In what follows, γ_{opt} will either denote $\hat{\gamma}$ or $\bar{\gamma}$.

C. Algorithm for Modes Retrieval

In our framework, we will consider that a mode is associated with a set of intervals, each corresponding to a particular time t. As for some t the number of detected modes may not be equal to the expected

number, we take this into account in our search for the modes. Our strategy to define the intervals associated with each mode is first to find the first time t_0 such that $\#(C_f(\gamma_{opt}, t_0)) = N_f(\Gamma)$, and then define $N_f(\Gamma)$ intervals at that time by considering for each j_k, $1 \leq k \leq N_f(\Gamma)$, in $C_f(\gamma_{opt}, t_0)$:

$$I_{j_k,t_0} \quad = \quad [j_k, \tilde{\jmath}_k] \ s.t. \ \forall j_k \leq j \leq \tilde{\jmath}_k \ |W_f(a_j, t_0)| > \gamma_{opt} \text{ and } |W_f(a_{\tilde{\jmath}_k+1}, t_0)| < \gamma_{opt}.$$

Each interval I_{j_k,t_0} is associated with one of the modes of the signal. Note that j_k depends on t_0 but we omit this dependancy for the sake of simplicity. Finally, we exploit the continuity of the wavelet transform with respect to t: the intervals detected at time t_0 should also be detected at the following time $t_0 + \Delta t$. Let us now explain how we compute the intervals $(I_{j_k,t_0+\Delta t})_k$ from the intervals $(I_{j_k,t_0})_k$. Three cases may occur:

- When $\#C_f(\gamma_{opt}, t_0 + \Delta t) = N_f(\Gamma)$, then we link the intervals at time $t_0 + \Delta t$ to those at time t_0, by following the criterion:

  $$I_{j_k,t_0} \text{ and } I_{j_k,t_0+\Delta t} \text{ belong to the same mode if } I_{j_k,t_0} \bigcap I_{j_k,t_0+\Delta t} \neq \emptyset.$$

  We then carry on considering the time $t_0 + \Delta t$ and the associated intervals.
- When $\#C_f(\gamma_{opt}, t_0+\Delta t) > N_f(\Gamma)$, then we get rid of irrelevant intervals by applying the following criterion:

  $$I_{j_k,t_0} \text{ and } I_{j_{\tilde{k}},t_0+\Delta t} \text{ belong to the same mode if } \tilde{k} = \underset{p}{\operatorname{argmax}} \left\{ |I_{j_p,t_0+\Delta t}|, \ s.t. \ , I_{j_k,t_0} \bigcap I_{j_p,t_0+\Delta t} \neq \emptyset \right\},$$

  where for an interval I, $|I|$ denotes its length. Doing so, we only consider at time $t_0+\Delta t$ the longer intervals that match those detected at time t_0. This technique enables us to define $N_f(\Gamma)$ intervals at time $t_0 + \Delta t$. We thus restart the procedure changing t_0 into $t_0 + \Delta t$ and considering just the defined set of intervals.
- When $\#C_f(\gamma_{opt}, t_0 + \Delta t) < N_f(\Gamma)$, for which we do not define any intervals $I_{j_k,t_0+\Delta t}$. Instead, we look for the first positive index l such that $\#C_f(\gamma_{opt}, t_0 + l\Delta t) = N_f(\Gamma)$. We then restart the procedure replacing t_0 by $t_0 + l\Delta t$ and by considering the associated intervals $I_{j_k,t_0+l\Delta t}$.

The same procedure is then applied from t_0 towards smaller times. We finally end up with either zero or $N_f(\Gamma)$ intervals associated with each t. We will see, in subsequent numerical applications, that the former happens when the wavelet representation is very bad locally. In such a case, it would be unwise to derive modes using the synchrosqueezing method. For each mode indexed by $1 \leq k \leq N_f(\Gamma)$, we can associate for most $t = q\Delta t$ an interval $I_{j_k,t} := [j_k, \tilde{\jmath}_k]$, which enables us to retrieve the modes by

considering the following reconstruction formula:

$$f_k(q\Delta t) = 2\mathcal{R}e\left[C_\Psi^{-1}\sum_{j\in I_{j_k,t}} W_f(a_j, q\Delta t)\frac{\log(2)}{n_v}\right]. \tag{18}$$

Doing so, we avoid both the problem of the binning of the frequency domain as well as the heuristic procedure involved in the determination of the modes (see section III-B). As already mentioned previously, the threshold γ_{opt} is computed to ensure good detection of the different modes. When reconstructing the modes using such a threshold leads to wavelet coefficients with a large amplitude being neglected. To improve the reconstruction, we comment that if the Fourier transform of Ψ is compactly supported inside $[\xi_\Psi - \Delta, \xi_\Psi + \Delta]$, then basically the scales of interest for the mode k at time t are $[\frac{\xi_\Psi - \Delta}{\phi_k'(t)}, \frac{\xi_\Psi + \Delta}{\phi_k'(t)}]$. Invoking (11), the amplitude of the wavelet transform attains a local maximum when $a_j\phi_k'(t) = \xi_\Psi$. Then, if the Fourier transform of the wavelet is symmetric with respect to its peak frequency (which is the case with the bump wavelet), the wavelet representation is almost symmetric with respect to the scale a_j associated with the peak frequency, (this is true for pure harmonic signals and also for multicomponent signals provided (11) holds). Consequently a good estimation $\bar{\phi}_k'(t)$ of $\phi_k'(t)$ is obtained by considering $\frac{\xi_\Psi}{a_{j_0}}$ where a_{j_0} is the middle of the interval a_{j_k} and $a_{\tilde{\jmath}_k}$ which are the scales associated with the indices j_k and $\tilde{\jmath}_k$ of the interval $I_{j_k,t}$. This then leads us to an alternative reconstruction formula:

$$f_k(q\Delta t) = \frac{2}{C_\Psi}\mathcal{R}e\left[\sum_{a_j\in J_{k,q}} W_f(a_j, q\Delta t)\frac{\log(2)}{n_v}\right], \tag{19}$$

where $J_{k,q} = [\frac{\xi_\Psi - \Delta}{\phi_k'(q\Delta t)}, \frac{\xi_\Psi + \Delta}{\phi_k'(q\Delta t)}]$. We investigate in the next section the relevance of the reconstruction formula (19) and we will also put forward its potential interest for signal sampling and denoising in section VII.

<u>Remark:</u> We should also note that the proposed procedure is also valid when the STFT is used instead of the wavelet transform.

VI. Illustrations of the Reconstruction Procedure and Comparisons

In this section, we compare some examples to illustrate the advantage of using the reconstruction approach described in (19) as opposed to that proposed in section III-B and which was implemented in [1]. Furthermore, we will compare the proposed method to EMD which consists in extracting the modes by analyzing the signal in the time domain [8].

A. Synchrosqueezing Frequency Modulated Multicomponent Signals

To illustrate the reconstruction procedure defined in (18) and (19), we consider the retrieval of the components of a modulated frequency signal $\sin(3(2\pi\times 77t + 30\sin(3\pi t))) + \sin(3(2\pi\times 46t + 21\sin(3\pi t))) +$

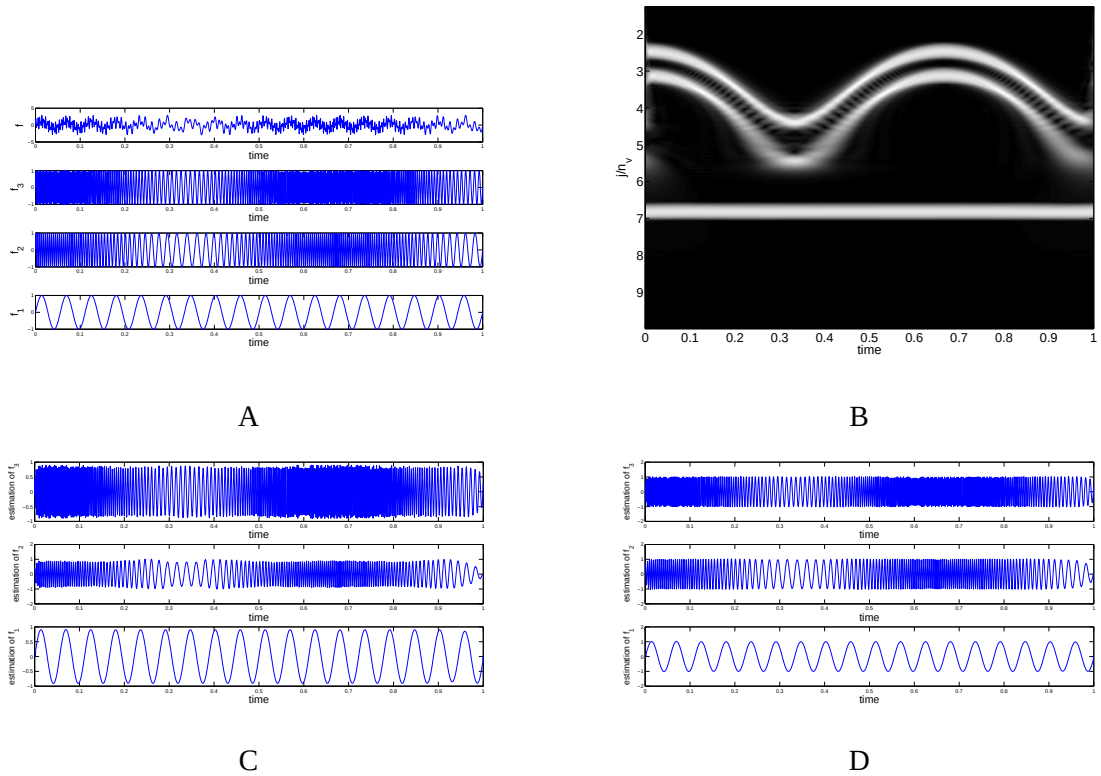

Fig. 4: A: An example of a signal made of the superposition of non trivial IMTs. B: corresponding wavelet representation. C: reconstruction of the modes of the signal in A using formula (18) and the bump wavelet ($\mu = 1$ and $\sigma = 0.2$); D: same as in A but using the reconstruction formula (19)

$\sin(3(2\pi \times 6t))$ (see Figure 4 A), which has a frequency separation condition $d \approx 0.2$ (see Definition 1). This signal admits the wavelet representation in Figure 4 B, computed using the bump wavelet with $\mu = 1$ and $\sigma = 0.2$. We test the two reconstruction methods (18) and (19) on the signal with the results depicted in Figure 4 C and D respectively. The mean square error (expressed in dB) associated with the reconstruction of the three modes f_1, f_2 and f_3 of Figure 4 A is 13.37 dB, 11.03 dB and 19.64 dB for (18) and 21.6 dB , 14.45 dB and 31.32 dB for (19). Note also that, in such a case, since $\hat{\gamma}$ exists we have a reconstruction formula for each time t.

Now, we wish to compare the procedure we propose for reconstruction to that introduced in section III-B. First, we remark that formula (9) proposed for reconstruction requires the knowledge of the number of modes. Even if the latter is known the determination of the optimal curves c^* is very sensitive to the choice of the parameter λ. To ensure a fair comparison, we compute formula (9) for the signal of Figure 4

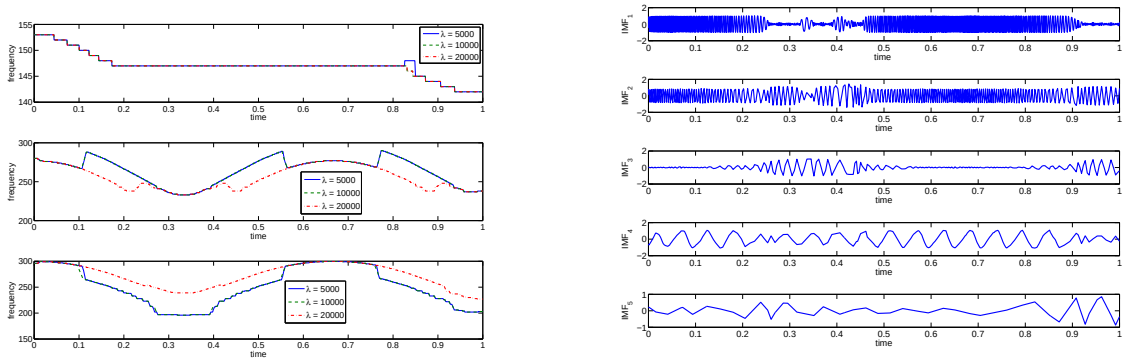

A B

Fig. 5: A: The optimal curves c^*, for different values of λ, B: The results of the EMD decomposition on the signal of Figure 4 A

A using the bump wavelet as analyzing wavelet still with $\mu = 1$ and $\sigma = 0.2$, and then display the optimal curves $c*$ depending on the value of λ on Figure 5 A (the tested values are $\lambda = 5.10^3$, 10^4 and 2.10^4). For larger λ, we note that the regularization term prevails over the synchrosqueezing term and some c^* being straight lines. Then, considering Figure 5 A is very informative on the way the reconstruction formula (9) works for smaller λ. Indeed, the algorithm selects in this case optimal curves made of several parts that belong to different frequency bands because the synchrosqueezing part prevails in the reconstruction formula, i.e. it creates mode-mixing. For instance, if one considers the value $\lambda = 2.10^4$, we see that for some times (typically between 0.3 and 0.4) the two optimal curves correspond to the same frequency band. We also note that the lack of precision in the determination of the optimal curves results in the modes obtained not summing up to the original signal.

Another technique used to represent such signals is EMD [8]. The main principle of the technique is to extract less and less oscillatory components from a signal by applying an iterative procedure called the sifting process (for further details on the method see [8]). We apply the EMD algorithm using the version given in [12] using the default parameters to the signal of Figure 4 A. The components of the decomposition, called IMFs (intrinsic mode functions), sum up to the original signal. In the present case, most of the energy of the original signal is contained in the first five IMFs which we depict on Figure 5 B. We notice that mode-mixing is present by considering IMF_1 and IMF_2, and note that the information contained in the modes f_3 and f_2 spreads over IMF_1, IMF_2 and IMF_3. Similarly, the information contained

in f_1 spreads over IMF_4 and IMF_5. The reason for such mode-mixing effects is related to the fact that the extraction of the IMFs in the EMD is not frequency based in contrast to the synchrosqueezing technique. Furthermore, we also comment that if an error is made in the extraction of the first IMF then it will spread throughout the whole extraction procedure. A deeper analysis of Figure 5 B, for $t < 0.2$, tends to show that EMD is relatively good at separating high frequency components but when the frequency modulation is important towards lower frequencies, it seems to need a stronger frequency separation condition than that involved in the study of synchrosqueezing (typically for $0.35 < t < 0.45$). This remark offers some insight to the study carried out in [6] on a two tone signal, which concluded that when the modes have the same amplitude and for a given frequency ratio, the separation of the mode is easier to achieve with synchrosqueezing than with EMD.

B. Analysis of Linear Chirp

In this section, we provide another illustration of the method on the extraction of linear chirps. Our aim is on the one hand to compare the behavior of our method with existing methods, namely EMD [8] and another version of the synchrosqueezing algorithm [1] and also to focus on the importance of the wavelet choice in the synchrosqueezing technique when ϵ is large.

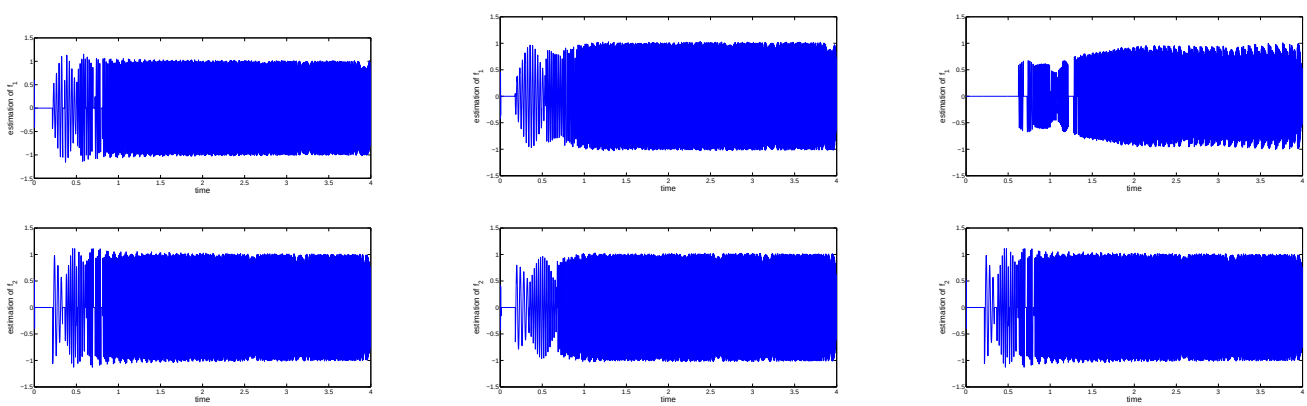

Fig. 6: The first row contains the estimation of f_1 using the reconstruction formula (19) with analyzing wavelet the bump wavelet with $\sigma = 0.02$ and $\mu = 0.2$, $\mu = 0.3$ and $\mu = 0.5$ from left to right. The second row contains the estimation of f_2 with the same parameters with regards to the wavelet transform

To do so we analyze the linear chirp signal $\cos(2\pi * 30 * (t + 1/4)^2) + \cos(2\pi * 24.55 * (t + 1/4)^2)$ whose wavelet transform was explored in Figure 2. Figure 2 showed the importance of the location of

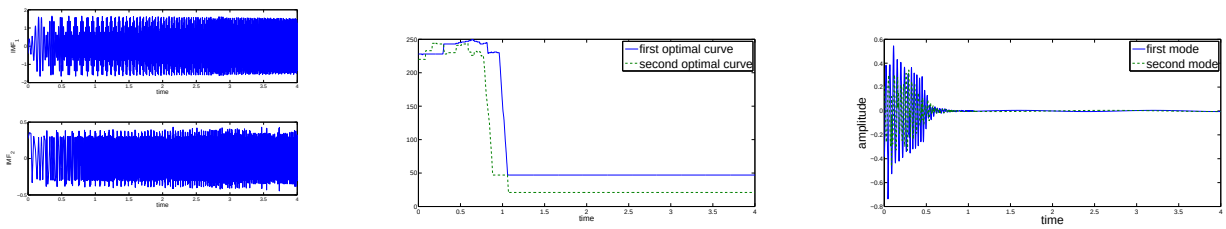

A B C

Fig. 7: A:The first two IMFs associated with the decomposition of the linear chirp, B: the two optimal curves given by the formula (9) with $\lambda = 1000$, C: the corresponding modes

the frequency center of the analyzing wavelet in terms of the quality of the representation. In the present case, we showed that ξ_Ψ had to be lower than 0.5 so that the estimation (11) could be reasonably good. Also it appeared that by moving the frequency center of the analyzing wavelet towards zero, a better time-scale resolution resulted. We now investigate how this improvement in the wavelet representation impacts the synchrosqueezing transform. We use the reconstruction formula (19) as suggested by the previous simulations on frequency modulated multicomponent signals again using the bump wavelet for analysis. Our simulations consist in moving the frequency center of the wavelet towards 0 by considering successively $\mu = 0.5$, $\mu = 0.3$ and $\mu = 0.2$, σ being fixed ; because we also have the constraint $\sigma \leq \mu d$ and since $d = 1/10$, we consider $\sigma = 0.02$ so that the previous inequality is valid for $\mu = 0.2$.

The results of Figure 6 show that by improving the approximation (11) for small t, the synchrosqueezing representation is greatly improved. Note that when the reconstruction formula returns zero this means that our algorithm is not able to separate the mode from the wavelet representation and we find it wiser not to propose any decomposition in such cases: when the analysis tools are inefficient this should be explicit. The rationale underlying this view is to make the most of the wavelet decomposition without extrapolating when the information is unclear. To measure quantitatively the improvement in the mode reconstruction brought about by the change in the frequency center of the wavelet, we compute the mean square error (measured in dB) associated with the reconstruction of the two modes either considering only the time indices such that $t > 0.8$ ($t > 0.8$ in Table I). Our basic insight is that better reconstruction is achieved for smaller times by moving the frequency center of the wavelet towards 0, which is confirmed by the results of Table I. This point is to our mind worth noting since it illustrates that the synchrosqueezing technique can be efficient in practice only when the analyzing wavelet is appropriately chosen. Note

also, that we had remarked earlier that to move the frequency center towards 0 worsens the wavelet representation for large t in the sense that its spreads the information over a larger number of scales. However, as the reconstruction procedure takes into account the location of the frequency center, it has no impact on the quality of the estimation of the modes.

	$\sigma = 0.02$ $\mu = 0.2$ $t > 0.8$	$\sigma = 0.02$ $\mu = 0.3$ $t > 0.8$	$\sigma = 0.02$ $\mu = 0.5$ $t > 0.8$
SNR (in dB,f_1 estimate)	21.4	18.53	-2.17
SNR (in dB,f_2 estimate)	21.17	16.82	-2.21

TABLE I: Influence of the location of the frequency center on the quality of the estimation of the modes using the synchrosqueezing transform

We are also concerned with comparing our method for mode extraction to the EMD and to the technique of extraction of the modes given by (9). For EMD, the useful information is mainly contained in the first two IMFs, which are displayed in Figure 7 A. The reconstruction error (measured in dB) is for the first and second modes (considering times larger than $t > 0.8$ to ensure a fair comparison with the synchrosqueezing technique) 2.09 dB and 2 dB respectively. Again, as EMD does not analyze the signal in the frequency domain it seems to be inefficient at separating components with close frequency characteristics. Now, to test formula (9) we still consider the decomposition of the linear chirp signal with the bump wavelet taking $\mu = 0.2$ and $\sigma = 0.02$. We notice that it clearly fails to reconstruct the modes because trying to determine two modes from the smallest time it becomes trapped by the poor representation given by the wavelet transform at these times. Figures 7 B and C illustrate this point for $\lambda = 1000$, other values of λ would offer no improvement.

VII. Signal Sampling and Denoising using Synchrosqueezing

A. Multicomponent Signals Sampling and Synchrosqueezing

Based on the previous study, we now investigate how to use the SM to determine relevant signal samples. Before getting into the technique we should briefly emphasize what motivates our study. The central paradigm of modern signal processing is the Nyquist-Shannon theorem which states that any signal f admitting a compactly supported Fourier transform included in $[-\Omega, \Omega]$ can be reconstructed from its regular samples through: $f(t) = \sum_{n\in\mathbb{Z}} f(n\frac{\pi}{\Omega})\text{sinc}(\Omega(t - n\frac{\pi}{\Omega}))$.

When one considers irregular samples as in [14], the reconstruction can be ensured provided the sampling points are a perturbation of regular sampling. More precisely if $T \leq 1/\Omega$ and if $t_k = \{Tk + a_k\}$ such that $\sup_k |t_k - Tk| < \frac{T}{2}$ then one can find out a series converging to f and based on these samples. The idea behind such a result is to determine uniform samples of f from the nonuniform samples $(f(t_k))_k$ and then use classical estimation on Fourier series. These kinds of representations based on the Fourier series do not take into account local signal frequency characteristics whereas it would be natural to relate the signal sampling to these characteristics. The approach we now describe is an attempt in this direction.

A study of the robustness of the SM to bounded perturbations when it is applied to a superposition of IMTs was given in [1]. In that study, the authors state that if $g = f + e$, where e is a small perturbation such that $\|e\|_{L^\infty} \leq C\epsilon$. Defining for all k, M_k as the largest real number such that $|\Phi_k'(t)| \in [M_k^{-1}, M_k]$, then the SM enables the reconstruction of f_k with an error of the order $M_k \epsilon^{1/3}$. From this we deduce that in such a case the SM enables a reconstruction of the signal f with an error of the order $\max_k M_k \epsilon^{1/3}$. In our following study, g will be an interpolant of f at some sample points and thus e will be the interpolation error. We aim at showing how the SM helps us find relevant samples by considering the interpolation error.

Let assume that g is obtained by sampling f at the points (t_m). Then if $D = \max_m |t_{m+1} - t_m|$, the interpolation error using cubic spline interpolant e is bounded by $\|e\|_{L^\infty} \leq \frac{5}{584} D^4 \|f^{(4)}\|_{L^\infty}$. Note also that by applying piecewise cubic Hermite interpolant instead, the upper bound for the interpolation error is even much lower, since we have: $\|e\|_{L^\infty} \leq \frac{1}{384} D^4 \|f^{(4)}\|_{L^\infty}$, which suggests that given a set of samples (t_m), a better reconstruction of the modes through synchrosqueezing (and consequently of the signal) should be achieved by using piecewise cubic interpolant. However, writting the upper bound of the error as previously wipes up the locality of the error estimation. Indeed, we had rather write when the piecewise cubic interpolant is used:

$$\|e\|_{L^\infty} \leq \frac{1}{384} \max_m \left\{ (t_{m+1} - t_m)^4 \|f^{(4)}\|_{L^\infty, [t_m, t_{m+1}]} \right\}, \tag{20}$$

which means that where $f^{(4)}$ is large, the sampling points should be close.

We aim to show that the extrema of the high frequency component obtained after synchrosqueezing are more relevant than the extrema of the signal itself in terms of the preservation of the signal frequency content after sampling. Indeed let us consider the following two signal reconstruction procedures. The first (resp. second) one consists in considering the extrema of the high frequency mode given by the SM (resp of the original signal) and then piecewise cubic Hermite interpolation of the original signal at these points (adding the first and the last point as interpolation points).

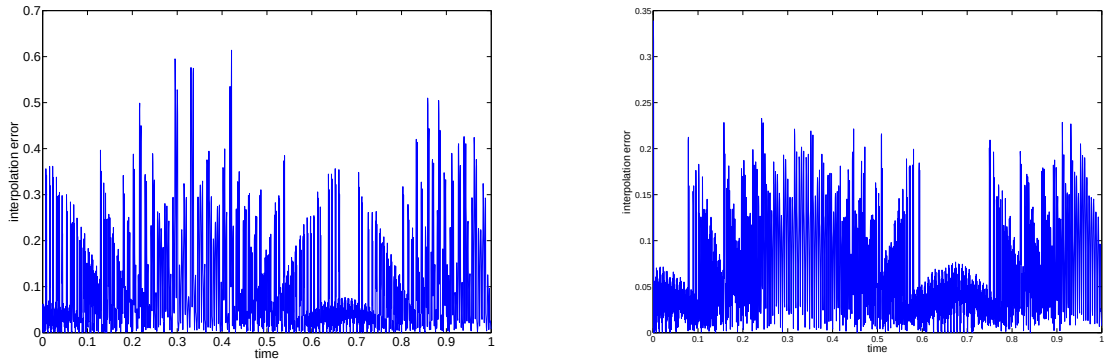

A B

Fig. 8: A:display of the function $t \to \sum_m \frac{1}{384}(t_{m+1}-t_m)^4|f^{(4)}(t)|\chi_{[t_m,t_m+1[}(t)$, where f is the signal of Figure 4 A and t_m are the extrema of the original signal, B: same computation where t_m are the extrema of the high frequency mode obtained after synchrosqueezing. Note the difference in the interpolation error changing the interpolation points

As an illustrative example, we again consider the signal of Figure 4 A to which we apply the SM using the same parameters as previously. Each method leads to 464 extrema points. The Nyquist frequency associated 500 Hz and the Nyquist-Shannon representation would lead to 1000 equally-spaced points on $[0,1]$. The time-scale representation of the interpolants being satisfactory, this suggests that the sampling should be based on local frequency and not on maximal frequency computation. Going further, we assess the quality of the two types of interpolant by computing the function $t \to \sum_m \frac{1}{384}(t_{m+1}-t_m)^4|f^{(4)}(t)|\chi_{[t_m,t_m+1[}(t)$. We notice that the amplitude of this function is much smaller when the extrema of the first mode after synchrosqueezing is used instead of those of the original signal (compare Figure 8 A and B). This suggests that the value of the signal at the extrema location of the first mode given by the SM is more relevant than the value of the signal at its extrema location in terms of frequency content. In spite, the numerical simulations proposed here is very limited the obtained results are encouraging and will be the subject for further developments.

B. Denoising with Synchrosqueezing

In this subsection we show that the SM enables us to define a denoising algorithm that outperforms the traditional wavelet denoising technique.

We first note that by computing the threshold γ_{opt} and by considering the wavelet coefficients whose amplitude are above that threshold, we perform wavelet thresholding even if we use formula (19). Our point is to show that the algorithm we have proposed to compute the mode is a very efficient tool for the denoising of multicomponent signals. We again consider the multicomponent signal which we previously studied for signal sampling to which we add a Gaussian white noise with a varying standard deviation. We then compute the SNR before denoising between the original and noisy signals. Then, we apply our synchrosqueezing algorithm to the noisy signal (still considering the bump wavelet with $\mu = 1$ and $\sigma = 0.2$ as in the noise-free case) and we obtain the so-called denoised signal by summing up all of the modes obtained. We finally compute the SNR after denoising between the denoised and the original signals and plot these in Figure 9. The SNR after denoising versus the SNR before denoising (curve labelled SR for Synchrosqueezing Reconstruction on that Figure). We now compare the behavior of our novel denoising technique to traditional wavelet thresholding techniques. We decompose our signal with a symmlet having six null moments and the depth of decomposition is set to three (denoted by WD for ”wavelet decomposition”, on Figure 9). We apply soft or hard thresholding techniques (ST and HT on Figure 9 respectively, using the classical estimation of the standard deviation of the noise [5]) on either the first or the first two levels of decomposition (1 scale or 2 scales on Figure 9 respectively). On such a multicomponent signal, the synchrosqueezing reconstruction algorithm preserves much better the characteristics of the original signal.

We believe that our algorithm behaves better for the reason that the wavelet coefficients of a modulated frequency mode can belong to several octaves and are thus thresholded differently depending on the time while the thresholding procedure embedded in the SM is the same whatever the frequency content of the mode. In future work, we will certainly address this issue in more detail but it is beyond the scope of the current paper.

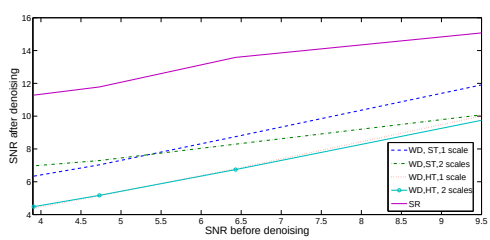

Fig. 9: SNR after denoising as a function of the SNR before denoising as a function either using the synchrosqueezing reconstruction technique (SR) or with various wavelet thresholding techniques (WD)

VIII. Conclusion

In this paper, we have presented a novel algorithm for the synchrosqueezing method. After emphasising the importance of the accuracy of the wavelet representation on which the synchrosqueezing algorithm is based, we then profited from the structure of the wavelet transform of multicomponent signals to develop a novel algorithm. We then showed that with regard to the mode-mixing issue, the proposed algorithm behaves better than EMD or any other existing implementation of the synchrosqueezing method. We then showed that in the noise-free configuration the proposed algorithm can be used to find out an appropriate sampling of multicomponent signals which no longer obey the constraints of the Shannon-Nyquist Theorem. Finally we showed that the algorithm also provides a natural way to denoise multicomponent signals and which outperforms classical wavelet thresholding techniques on these signals. Future work requires a deeper study of the denoising and sampling procedure provided by the synchrosqueezing method along with some new developments on synchrosqueezing-like techniques especially when the wavelet representations are not accurate enough. Finally, we are very concerned in future work with developing a better mathematical formulation of the proposed reconstruction algorithm.

References

[1] E. Brevdo, N. S. Fuckar, G. Thakur, H-T. Wu, *The Synchrosqueezing Algorithm: a Robust Analysis Tool for Signals with Time-Varying Spectrum,* submitted, 2011, arXiv id: 1105.0010.

[2] R. A. Carmona, W.L. Hwang, and B. Torrésani, *Multiridge Detection and Time-Frequency Reconstruction,* IEEE Transactions on Signal Processing, vol. 47, no. 2, pp. 480-492, 1999.

[3] E. Chassande-Mottin, I. Daubechies, F. Auger and P. Flandrin, *Differential Reassignment,* IEEE Signal Processing Letters, vol. 4, no. 10, pp. 293-294, 1997.

[4] I. Daubechies, J. Lu and H-L. Wu, *Synchrosqueezed Wavelet Transforms: an Empirical Mode Decomposition-Like Tool,* Applied and Computational Harmonic Analysis, vol. 20, no. 2, pp. 243-261,2011

[5] D.L. Donoho, I.M. Johnstone, *A*dapting to Unknown Smoothness via Wavelet Shrinkage JASA, vol 90, 432, pp. 1200-1224, 1995

[6] P. Flandrin and P. Borgnat, *Time-Fequency Energy Distributions Meet Compressed Sensing,* IEEE Transactions on Signal Processing, vol. 58, no. 6, pp. 2974-2982, 2010

[7] H-T. Wu, P. Flandrin and I. Daubechies, *One or Two Frequencies? The Synchrosqueezing Answer,* Advances in Adaptive Data Analysis, vol. 3,no.1-2, pp. 29-39, 2011

[8] N.E. Huang, Z. Shen, S.R. Long, M.C. Wu, H.H. Shin, Q. Zheng, N-C. Yen, C. C. Tung and H.H. Liu, *The Empirical Mode Decomposition and Hilbert Spectrum for Nonlinear and Non-Stationary Time Series Analysis,* Proceedings of the Royal Society of London, vol. 454, pp. 903-995, 1998.

[9] J.M. Lilly and S.C. Olhede, *On the Analytic Wavelet Transform,* IEEE Transactions on Information Theory, vol. 56, no. 8, pp. 4135-4156, 2010.

[10] S. Mallat, *A Wavelet Tour on Signal Processing,* Academic Press, 1998.

[11] S. Olhede and A.T. Walden, *The Hilbert Spectrum via Wavelet Projections,* Proc. R. Soc. Lond. A, vol. 460, pp. 955-975, 2004.

[12] G. Rilling, P. Flandrin and P. Goncalves, *On Empirical Mode Decomposition and its Algorithms,* IEEE-EURASIP Workshop on Nonlinear Signal and Image Processing, NSIP-03, Grado (I), June 2003.

[13] X. Rodet and P. Depalle, *A New Additive Synthesis Method Using Inverse Fourier Transform and Spectral Envelope,* In Proc. ICMC, San Jose, 1992.

[14] G. Thakur and H-T. Wu, *Synchrosqueezing-Based Recovery of Instantaneous Frequency from Nonuniform Samples,* SIAM J. Math. Analysis, vol.43, no. 5, pp. 2078-2095, 2011.